J Ther Eng, Vol. 11, No. 2, pp. 448−463, March, 2025

Journal of Thermal Engineering
Web page info: https://jten.yildiz.edu.tr
DOI: 10.14744/thermal.0000926

Research Article

Stability analysis of the mixed convective flow of Jeffrey nanofluid through a porous medium

Harsha S. V.[1], **Chandra Shekara Guruva REDDY**[2,*], **Hemanth Kumar C.**[2]

[1]*Department of Mathematics, FET, Jain Deemed-to-be University, Bangalore, 562112, India*
[2]*Department of Mathematics, VTU Research Center, BMS College of Engineering, Bangalore, 560019, India*

ARTICLE INFO

Article history
Received: 16 January 2024
Revised: 28 April 2024
Accepted: 10 June 2024

Keywords:
Horizontal Pressure Gradient; Instability; Jeffrey Fluid; Mixed Convection; Nanofluid; Porous Layer

ABSTRACT

This study investigates the stability of a mixed convective flow of a nanofluid through a horizontal porous layer using an unsteady Jeffrey-Darcy model. Linear stability theory is employed to assess the stability of a system, where the base fluid is modeled as a Jeffrey fluid with dispersed nanoparticles in a state of thermal equilibrium. The stability equations are derived as an eigenvalue problem using Fourier decomposition, solved using the higher order Weighted Residual Galerkin Method (WRGM), and validated analytically. The results are presented in terms of critical values of the Darcy-Rayleigh number, wave number, and wave speed over nondimensional parameters. Further, the impact of nondimensional numbers like horizontal pressure gradient, thermal diffusivity ratio, and nanoparticle volume fraction has stabilizing effects, whereas the Jeffrey parameter and the Vadasz number have the opposite effect. Moreover, it has been observed that the increase in the Jeffrey parameter reduces the stability region. The variation Jeffrey parameter causes a change in the flow and thereby discards the analytical proof of stability even under the limit of an infinite Vadasz number. The inquiry into the stability or instability of the fundamental flow is addressed by solving the eigenvalue problem numerically over a finite range of the Jeffrey parameter and horizontal pressure gradient. These results indicate that the oscillatory convection mode is advantageous for estimating the required volume fraction of nanoparticles in the base fluid to improve the thermal efficiency of Jeffrey nanofluids. Numerical and graphical analyses explore the impacts of dimensionless parameters on physical systems, providing insights into the system's stability properties under varying conditions.

Cite this article as: S. V. H, Reddy CSG, C. HK. Stability analysis of the mixed convective flow of Jeffrey nanofluid through a porous medium. J Ther Eng 2025;11(2):448−463.

INTRODUCTION

Mixed convective flows of non-Newtonian fluids represent a complex and fascinating area of study in fluid dynamics. These fluids, which include various types such as polymer solutions, slurries, and biological fluids, exhibit behaviors that deviate from the classic Newtonian fluid model. In mixed convective flows, the fluid motion

***Corresponding author.**
*E-mail address: chandrashekarag.maths@bmsce.ac.in

This paper was recommended for publication in revised form by Editor-in-Chief Ahmet Selim Dalkılıç

is influenced by both buoyancy forces due to temperature gradients and external forces or pressures. Understanding the behavior of mixed convective non-Newtonian fluids is crucial in many industrial processes, such as polymer processing, food processing, and oil recovery. Researchers and engineers often employ advanced numerical simulations and experimental techniques to unravel the intricate dynamics of these fluids and optimize processes for efficiency and performance. Understanding mixed convection in porous media is essential for geothermal reservoirs, underground energy storage, nuclear reactors, and solar collector applications. Prasad et al. [1] investigated mixed convection in horizontal porous layers heated from below, shedding light on heat transfer mechanisms in such systems. Sphaier and Barletta [2] explored unstable mixed convection in a heated horizontal porous channel, highlighting the importance of understanding flow instabilities in porous media systems. Ozgen and Varol [3] conducted a numerical study of mixed convection in a channel filled with a porous medium, providing valuable insights into heat transfer phenomena in porous media through computational simulations. These studies collectively enhance our understanding of mixed convection in porous media and its implications for various engineering and environmental applications. Vafai [4] provided a comprehensive reference for researchers, covering various aspects of porous media and its applications. Kim and Vafai [5] studied the use of nanofluids to enhance buoyancy-driven heat transfer in porous enclosures, demonstrating the potential of nanofluids to enhance heat transfer in porous media. Abu-Nada and Chamkha [6] provided insights into the effect of solid boundaries on mixed convection in a lid-driven cavity filled with a fluid-saturated porous medium. Nield and Bejan [7] provided a comprehensive overview of convection in porous media, emphasizing its importance in various engineering applications. Ingham and Pop [8] further advanced the understanding of transport phenomena in porous media, focusing on theoretical and experimental aspects. Nield [9] contributed to the development of boundary conditions for porous media simulations with a porous medium model with the Navier slip boundary condition. A study by Postelnicu [10] examined mixed convective instability due to the effect of a horizontal pressure gradient and temperature difference for the Newtonian fluids on the onset of Darcy-Bénard convection in thermal non-equilibrium conditions, revealing insights into the interplay between pressure gradients and thermal non-equilibrium, thus elucidating the mechanisms governing convective flow in porous media.

On the other hand, the significance of nanofluids has gained recognition alongside the research conducted, as evidenced by the following studies. Buongiorno [11] studied convective transport in nanofluids. The study by Choi et al. [12] investigates the unusual increase in thermal conductivity observed in nanotube suspensions, a phenomenon with significant implications for various technological applications. An investigation conducted by Mostafizur et al. [13] aimed to quantify the thermal conductivity of methanol-based nanofluids (MBNF) and demonstrated that nanoparticle clustering is the primary factor contributing to enhanced thermal conductivity. Tzou [14] investigated the thermal instability of nanofluids in natural convection. Nield and Kuznetsov [15] analyzed thermal instability in a porous medium layer saturated by a nanofluid. Kuznetsov and Nield [16] discussed the effect of local thermal non-equilibrium on the onset of convection in a porous medium layer saturated by a nanofluid. Bhaduria and Agarwal [17] studied convective transport in a nanofluid-saturated porous layer with a thermal non-equilibrium model. Chand and Rana [18] discussed the oscillating convection of nanofluid in a porous medium. Yadav et al. [19] analyzed the onset of convection in a binary nanofluid-saturated porous layer. Yadav et al. [20] discussed thermal convection in a Kuvshiniski viscoelastic nanofluid-saturated porous layer. Sheu [21] analyzed the linear stability of convection in a viscoelastic nanofluid layer. Chand et al. [22] discussed the thermal instability analysis of an elastic-viscous nanofluid layer. Recent studies have advanced nanofluid behavior comprehension and thermal performance improvement across diverse applications, while additional research has focused on refining analytical and numerical techniques in thermal transport [23-32] and these studies offer insights into thermal performance improvement in engineering.

Many studies have explored the behavior of Jeffrey fluid in porous media, some of which are summarized below. Nadeem and Akbar [33] analyzed the peristaltic flow of a Jeffrey fluid with variable viscosity in an asymmetric channel. Nallapu et al. [34] investigated the flow of a Jeffrey fluid through a porous medium in narrow tubes. Yadav [35] examines the influence of anisotropy on Jeffrey fluid convection in horizontal rotary porous layers, enhancing our understanding of convective heat transfer in anisotropic porous media. Naganthran [36] studied the effects of heat generation/absorption in Jeffrey fluids flowing past permeable stretching/shrinking discs, providing valuable insights into viscoelastic fluid behavior in thermal gradients.

Numerous studies have been conducted to investigate free convection in Jeffrey nanofluids through porous media. The study of Jeffrey nanofluid convection in porous media has enhanced heat transfer efficiency and energy conservation in diverse applications. By leveraging the unique properties of Jeffrey fluids and the heat transfer characteristics of nanoparticles, these fluids exhibit superior heat transfer performance compared to conventional fluids. They are particularly beneficial in applications where efficient heat transfer is crucial, such as cooling systems, thermal management, and heat exchangers. Moreover, Jeffrey nanofluids can improve energy efficiency, reduce environmental impact, and enhance stability in high-temperature environments. These attributes underscore the promising nature of research in Jeffrey nanofluid convection in porous media, with significant potential for practical applications across

various fields. For instance, Zhang et al. [37] explored the thermal behavior of Jeffrey nanofluid flow in a porous medium with a convective boundary condition. This study Siddiqui et al. [38] investigates the influence of Darcy and Prandtl numbers on the unsteady heat transfer characteristics of Jeffrey nanofluid flowing through a porous medium. Sharma et al. [39] investigated thermal convective instability in a Jeffrey nanofluid saturating a porous medium under rigid-rigid and rigid-free boundary conditions. Recent work by Pushap et al. [40] explored the thermal instability of rotating Jeffrey nanofluids in porous media with variable gravity, highlighting the importance of understanding their stability for optimizing heat transfer processes in engineering applications. Gautam et al. [41] investigate stationary convection in the electrohydrodynamic thermal instability of Jeffrey nanofluid layers saturating porous media under different boundary conditions, furthering our understanding of nanofluid dynamics. Shehzad et al. [42] studied the MHD flow of a Jeffrey nanofluid with convective boundary conditions. Shahzad et al. [43] studied the numerical simulation of magnetohydrodynamic Jeffrey nanofluid flow and heat transfer over a stretching sheet considering Joule heating and viscous dissipation. Sreelakshmi et al. [44] analyzed the homotopy analysis of a Jeffrey nanofluid's unsteady flow heat transfer over a radially stretching convective surface. Devi et al. [45] explores the behavior of electroconvection in a rotating Jeffrey nanofluid saturating a porous medium under different boundary conditions, with implications for applications in fields like microfluidic devices and geophysics. Promila Devi et al. [46] explore the initiation of thermal instability within a Darcy–Brinkman porous layer containing a Jeffrey nanofluid under rotation, offering a novel perspective on heat transfer processes in non-Newtonian fluids with potential applications in improving industrial system efficiency. Sharma et al. [47] investigate the impact of a magnetic field on thermosolutal convection in a Jeffrey nanofluid with a porous medium, employing linear stability analysis and the Darcy model. Maatoug et al. [48] explores the applications of the thermos-diffusion effect in the context of squeezing flow of Jeffrey nanofluids through a horizontal channel, highlighting the influence of inertial effects, Darcy-Forchheimer flow, viscous dissipation, and activation energy, with a focus on numerical computations and physical flow parameters. Sushma et al. [49] discussed the mixed convection flow of a Jeffrey nanofluid in a vertical channel.

Current studies have shed light on the intricate dynamics of mixed convective flows in porous media, particularly focusing on the interplay between pressure gradients and viscoelastic fluid behavior. Additionally, Pallavi et al. [50] explore oscillatory Darcy-Bénard-Poiseuille mixed convection by extending the work Postelnicu in an Oldroyd-B fluid-saturated porous layer. It investigates flow and thermal behavior through theoretical analysis and numerical simulations of pressure gradients. The study contributes to understanding complex fluid dynamics in porous media for practical applications. In a related study to Postelnicu, Hemanthkumar and Shivakumara [51] studied the thermal instability of an Oldroyd-B fluid-saturated porous layer, incorporating considerations of pressure gradients and LTNE temperatures, thus providing insights into the thermal behavior of viscoelastic fluid flows in porous media and highlighting the role of pressure gradients and temperature differentials in driving mixed convective instabilities.

Despite extensive research on the onset of instability in natural, forced, or mixed convection within a horizontal porous layer involving Newtonian or non-Newtonian fluids or nanofluids, there is a significant gap in the literature regarding the contribution of similar works, including horizontal pressure gradient effects, to the study of mixed convection in a porous layer saturated with a Jeffrey nanofluid. This gap has led to novel investigations exploring the effects of horizontal pressure gradient and buoyancy due to temperature differences on mixed convection in such a porous layer. Our study aims to investigate the influence of the Jeffrey parameter and other factors on the instability of stationary and oscillatory convection in a porous layer, focusing on the thermal applications of Jeffrey nanofluids. By examining the linear stability in mixed convection of Jeffrey's nanoporous fluid, we aim to deepen our understanding of how porosity and nanoparticle characteristics impact the onset of convection. This research is particularly relevant in industries such as food processing and electronics cooling, providing insights into low-volume fraction and low-permeable porous channels, which are crucial for managing and enhancing convection. Using linear stability theory, we identify key factors influencing convective motion, as detailed in the following sections.

MATHEMATICAL FORMULATION

The two-dimensional rectangular coordinate system (x, z) is chosen, where the x-axis is taken along the plates of the horizontal channel and the z-axis is perpendicularly upwards in which gravity $(\vec{g})$ is acting downwards. The plates at $z = d$ and $z = 0$ are maintained at dissimilar constant temperatures T_c and T_h respectively, with $T_h > T_c$ a porous matrix in between the plates. It is filled with -nanofluid which is heated from below and cooled from above as illustrated in Figure 1. The free and forced convection flow is due to the buoyant force with temperature difference $(\Delta T = T_h - T_c)$ and constant horizontal pressure gradient respectively leads to mixed convection flow.

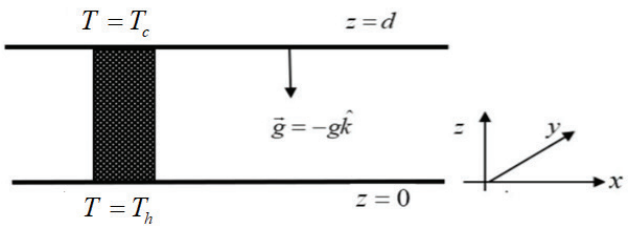

Figure 1. Physical configuration.

The following assumptions are made:

- A fully developed and non-quiescent base flow is assumed with an applied horizontal pressure gradient.
- Due to the low permeability of the porous channel, the unsteady Darcy model is adopted.
- The Boussinesq approximation $\rho = \rho_0 (1 - \beta (T - T_c))$ is used such that the density varies only with temperature.
- The nanoparticle volume fraction is considered to be low and constant [52].
- The study is restricted to linear stability along with normal mode analysis.
- The local thermal equilibrium between the fluid and solid phases holds in a porous medium.

Based on the aforementioned assumptions, the governing equations are formulated following the approach outlined by Yadav [35].

$$\nabla . \vec{q} = 0 \tag{1}$$

$$\frac{\rho_{nf}}{\varepsilon}\frac{\partial \vec{q}}{\partial t} = -\nabla P - \rho_{nf}\beta_{nf}(\mathrm{T} - T_c)\vec{\mathrm{g}} - \frac{\mu_{nf}}{K(1+\lambda)}\vec{q} \tag{2}$$

$$\sigma\frac{\partial T}{\partial t} + (\vec{q}.\nabla)T = \frac{k_{nf}}{(\rho C_p)_{nf}}\nabla^2 T \tag{3}$$

The corresponding boundary conditions are given by

$$\vec{q} = 0 \text{ at } z = 0 \text{ and } z = \mathrm{d}, \tag{4}$$

$$T = T_h \text{ at } z = 0 \text{ and } T = T_c \text{ at } z = d \tag{5}$$

Thermo-physical Properties of Nanofluids

The thermophysical properties of water-based nanofluid are used in the present study. The effective viscosity of the nanofluid, μ_{nf} is computed using the base fluid viscosity μbf and a diluted suspension of tiny sphere-shaped nanoparticles,

$$\mu_{nf} = \frac{\mu_{bf}}{(1-\phi)^{2.5}}, \tag{6}$$

The validation has been confirmed by [53] through experimental investigation utilizing oil-water nanofluids at temperatures ranging from 20 to 50 degrees Celsius. The subsequent experimental findings are in the [54] and discovered that it is completely consistent. The approximate thermal conductivity for the nanofluid is calculated using the [55] model. The model tells us, with the help of suspended nanoparticles how the thermal conductivity of nanofluid increases and is given by,

$$k_{nf} = k_{bf}\left[\frac{(k_{np} + 2k_{bf}) - 2\phi(k_{bf} - k_{np})}{(k_{np} + 2k_{bf}) + \phi(k_{bf} - k_{np})}\right] \tag{7}$$

At the reference temperature, the nanofluids effective density and heat capacitance are computed as [56] and [57] respectively as follows,

$$\rho_{nf} = (1-\phi)\rho_{bf} + \phi\rho_{np} \text{ and}$$
$$(\rho C_p)_{nf} = (1-\phi)(\rho C_p)_{bf} + \phi(\rho C_p)_{np}, \tag{8}$$

Following are the formulas for nanofluids volumetric expansion coefficient and thermal diffusivity for nanofluids respectively,

$$(\rho\beta)_{nf} = (1-\phi)\rho_{bf}\beta_{bf} + \phi\rho_{np}\beta_{np} \text{ and } \alpha_{nf} = \frac{k_{nf}}{(\rho C_p)_{nf}}. \tag{9}$$

A Jeffrey nano-fluid model with single-phase, which is suitable for low-volume quantities of nanoparticles, is used to explain the features of nano-fluids. The thermophysical properties of the several nanoparticles at ambient temperature are shown in Table 1 [52].

Table 1. Thermo-physical properties of nanoparticles

Physical properties	CuO	Al_2O_3	TiO_2
Cp (J/KgK)	531.80	765.00	686.20
ρ (Kg/m^3)	6320.00	3970.00	4250.00
k (W/mK)	76.50	40.00	8.95
$\alpha \times 10^7$ (m^2/s)	227.60	131.70	307.00
$\beta \times 10^5$ (1/K)	1.80	0.85	0.90

Non-dimensional Governing Equations

The physical quantities of length, velocity, time, pressure, and temperature of nanofluid in the governing equations (1)– (5) are made non-dimensionalized using the scales d, $\frac{\varepsilon\alpha_{bf}}{d}$, $\frac{d^2}{\alpha_{bf}}$, $\frac{\varepsilon\mu_{nf}\alpha_{bf}}{K}$ and ΔT respectively and the following dimensionless governing equations in the cartesian coordinates are obtained by

$$\nabla . \vec{q} = 0 \tag{10}$$

$$\frac{1}{V_a}\frac{\partial \vec{q}}{\partial t} = -\nabla P + q_1 R_D T\hat{k} - \frac{\vec{q}}{(1+\Lambda)} \tag{11}$$

$$\frac{\partial T}{\partial t} + (\vec{q}.\nabla)T = \alpha_1\nabla^2 T \tag{12}$$

where Λ is the nondimensional Jeffrey parameter, $R_D = \frac{\rho_{bf}\beta_{bf}K\,d\,g\,\Delta T}{\mu_{nf}\alpha_{bf}\varepsilon}$ is the Darcy-Rayleigh number, $q_1 = \frac{\rho_{nf}\beta_{nf}}{\rho_{bf}\beta_{bf}}$ is the nano-particle volume fraction ratio of nanofluid to base fluid, $\alpha_1 = \frac{\alpha_{nf}}{\alpha_{bf}}$ is the ratio of thermal diffusivity of nanofluid to base fluid, and $V_a = \frac{\mu_{nf}\varepsilon d^2}{K\alpha_{nf}}$ is the Vadasz number.

The corresponding dimensionless boundary conditions are given by

$$\vec{q} = 0 \text{ at } z = 0,1,\ T = 1 \text{ at } z = 0 \text{ and } T = 0 \text{ at } z = 1 \quad (13)$$

Linear Stability Analysis

The linear stability analysis of mixed convection assumes a non-quiescent basic state of fluid flow, influenced by a constant horizontal pressure gradient as described in the following form,

$$\vec{q}_b = (u_b, w_b) = (\Pi, 0),\ P = P_b(z) \text{ and } T = T_b(z). \quad (14)$$

The corresponding basic state solutions are given by

$$u_b = \Pi,\ T_b = 1 - z \text{ and } \mathrm{P}_b = \left(\frac{z^2}{2} - \mathrm{z}\right) q_1 R_D. \quad (15)$$

Further, we superimpose infinitesimally small perturbations on the basic state given in (15) in the form:

$$\vec{q} = \Pi i + \vec{q}',\ P = P_b(z) + P' \text{ and } T = T_b(z) + T' \quad (16)$$

The stability equations are derived by following a sequence of operations first we linearize equations (11) and (12) by substituting perturbed quantities given equation (16) then the pressure is eliminated by operating curl on the resultant equation ... and finally substituting stream function in the form $u = -\frac{\partial \psi}{\partial z}$ and $w = \frac{\partial \psi}{\partial x}$, we get

$$\left[\frac{1}{V_a}\frac{\partial}{\partial t} + \frac{1}{(1+\Lambda)}\right]\left(\frac{\partial^2 \psi}{\partial x^2} + \frac{\partial^2 \psi}{\partial z^2}\right) = q_1 R_D \frac{\partial T}{\partial x}, \quad (17)$$

$$\frac{\partial T}{\partial t} + \left\{\Pi \frac{\partial T}{\partial x} - \frac{\partial \psi}{\partial x}\right\} = \alpha_1 \nabla^2 T. \quad (18)$$

At this moment for a better understanding of the impact of all parameters on the wave number and frequency of perturbations, the solution of equations (17) and (18) are expressed in the form of normal modes given by

$$(\psi, T) = (\Psi(z), \Theta(z)) e^{ia(x - \omega t)} \quad (19)$$

where a is the wavenumber and $\omega = \omega_r + i\omega_i$ is the complex wave speed. The growth rate ω_i marks the difference between stability ($\omega_i < 0$) and instability ($\omega_i > 0$) . Substituting Eq. (19) in Eqs. (17) and (18), we obtain the following equations:

$$\left[\frac{1}{(1+\Lambda)} - \frac{ia\omega}{V_a}\right]\left(D^2 - a^2\right)\Psi - iaq_1 R_D \Theta = 0, \quad (20)$$

$$ia\Psi + \left[\alpha_1\left(D^2 - a^2\right) + ia\omega - \Pi ia\right]\Theta = 0. \quad (21)$$

The corresponding boundary conditions are given by

$$\Psi = 0 = \Theta \text{ at } z = 0 \text{ and } \Psi = 0 = \Theta \text{ at } z = 1. \quad (22)$$

Growth Rate Analysis

The classical integral method, as described by Shankar and Shivakumara [58], is utilized to analyze the thermal instability in the limit as V_a approaches infinity. First, we operate $(D^2 - a^2)$ on Eq. (21) to eliminate ψ and obtain the above equation for Θ in the form,

$$-a^2 q_1 (1+\Lambda) R_D \Theta + \alpha_1 \left(D^2 - a^2\right)^2 \Theta + ia\omega\left(D^2 - a^2\right)\Theta - \Pi ia\left(D^2 - a^2\right)\Theta = 0$$

Multiply $\bar{\Theta}$ the complex conjugate form of Θ and integrate with respect to z over the limit 0 to 1, which yields

$$-a^2 q_1 (1+\Lambda) R_D \int_0^1 \Theta\bar{\Theta}\,dz + \alpha_1 \int_0^1 \left(D^2 - a^2\right)^2 \Theta\bar{\Theta}\,dz + ia\omega \int_0^1 \left(D^2 - a^2\right)\Theta\bar{\Theta}\,dz - \Pi ia \int_0^1 \left(D^2 - a^2\right)\Theta\bar{\Theta}\,dz = 0$$

We apply integration by parts to the above equation, we arrive at the following equation,

$$-a^2 q_1 (1+\Lambda) R_D \int_0^1 |\Theta|^2\,dz + \alpha_1 \int_0^1 \left(|\Theta''|^2 + 2a^2|\Theta'|^2 + a^4|\Theta|^2\right)dz - ia\omega \int_0^1 \left(|\Theta'|^2 + a^2|\Theta|^2\right)dz + \Pi ia \int_0^1 \left(|\Theta'|^2 + a^2|\Theta|^2\right)dz = 0 \quad (23)$$

By evaluating the real part of Eq. (23), we obtain

$$\omega_i = \frac{-a^2 q_1 (1+\Lambda) R_D \int_0^1 |\Theta|^2\,dz + \alpha_1 \int_0^1 \left(|\Theta''|^2 + 2a^2|\Theta'|^2 + a^4|\Theta|^2\right)dz}{-a \int_0^1 \left(|\Theta'|^2 + a^2|\Theta|^2\right)dz} \quad (24)$$

Thus, one may conclude that

(i) İf $a^2 q_1 (1+\Lambda) R_D \int_0^1 |\Theta|^2 dz < \alpha_1 \int_0^1 \left(|\Theta''|^2 + 2a^2 |\Theta'|^2 + a^4 |\Theta|^2 \right) dz$ then $\omega_i < 0$ indicating the system is stable, and

(ii) if $a^2 q_1 (1+\Lambda) R_D \int_0^1 |\Theta|^2 dz > \alpha_1 \int_0^1 \left(|\Theta''|^2 + 2a^2 |\Theta'|^2 + a^4 |\Theta|^2 \right) dz$ then $\omega_i > 0$ the system becomes unstable.

Method of Numerical Solutions

Equations (20) and (21) form a complex eigenvalue problem and are solved utilizing WRGM. In this method, the test (weighted) functions are the same as the base (trail) functions. Accordingly, $\Psi(z)$ and $\Theta(z)$ are expanded in a finite series of basis functions in the form,

$$\Psi = \sum_{i=1}^{N} A_i \Psi_i(z), \text{ and } \Theta = \sum_{i=1}^{N} B_i \Theta_i(z) \tag{25}$$

where A_i and B_i are constants while $\Psi_j(z)$ and $\Theta_j(z)$ are the basis functions and are generally chosen to satisfy the respective boundary conditions, respectively N represents the number of terms considered in the Galerkin expansion. The basis functions are described by the power series that adhere to the pertinent boundary conditions

$$\Psi_i = z^i - z^{i+1} = \Theta_i, \tag{26}$$

These series are substituted back into Equations (20) and (21) and the WRGM procedure of demanding that the residues be normal to the basis functions is applied by multiplying the resulting Eq. (20) by $\Psi_j(z)$ and Eq. (21) by $\Theta_j(z)$ integrating by parts with respect to z between $z = 0$ and $z = 1$, and the boundary conditions are used to obtain the following system of algebraic equations:

$$A_i E_{ji} + B_i F_{ji} = \omega A_i G_{ji} \tag{27}$$

$$A_i H_{ji} + B_i I_{ji} = \omega B_i J_{ji}, \tag{28}$$

the coefficients of E_{ji} and J_{ji} involve the inner products and are given by

$$\begin{aligned}
&E_{ji} = \frac{1}{1+\Lambda}\left[\langle D\Psi_j\, D\Psi_i\rangle - a^2 \langle \Psi_j\, \Psi_i\rangle\right],\\
&F_{ji} = -iaq_1 R_D \langle \Psi_j \Theta_i\rangle, \mathrm{G}_{ji} = \frac{ia}{V_a}\left[\langle D\Psi_j\, D\Psi_i\rangle - a^2 \langle \Psi_j\, \Psi_i\rangle\right],\\
&H_{ji} = ia\langle \Theta_j \Psi_i\rangle, \mathrm{I}_{ji} = -\left[\alpha_1 \langle D\Theta_j\, D\Theta_i\rangle + (\alpha_1 a^2 + ia\Pi)\langle \Theta_j \Theta_i\rangle\right],\\
&J_{ji} = -ia\langle \Theta_j \Theta_i\rangle.
\end{aligned} \tag{29}$$

where the inner product is defined by $\langle \ldots \rangle = \int_0^1 (\ldots) dz$ equations (27) and (28) can be written in the matrix form as

$$AX = \omega BX \tag{30}$$

Where

$$A = \begin{bmatrix} E_{ji} & F_{ji} \\ H_{ji} & I_{ji} \end{bmatrix}, B = \begin{bmatrix} G_{ji} & 0 \\ 0 & J_{ji} \end{bmatrix} \text{and } X = \begin{bmatrix} A_i \\ B_i \end{bmatrix}$$

Equation (30) forms a generalized eigenvalue problem in which that A and B are $2N \times 2N$ order complex matrices, X is the eigenvector and $\omega = \omega_r + i\omega_i$ is the complex eigenvalue.

The integral occurring in the coefficients of E_{ji} and J_{ji} are analytically evaluated to avoid errors during the numerical integration. The main stages of the numerical procedure involved in solving Eq. (30) are as follows

i) Among the $2N$ eigenvalues, we identify the most growing or the least decaying mode having the largest imaginary part of the eigenvalue ω and call that mode simply the most growing mode.
ii) The largest value of ω_i is now forced to zero by varying R_D for a fixed value of wave number a and other governing parameters.

The computational software program MATHEMATICA 11.3 (Wolfram Research) is used to provide an ideal platform for the execution of Both stages and the following built-in functions are used:

Max[*Im*[*Eigenvalues*[*A,B*]]]= *EV* (*say*) *and*
Find Root [*EV*[R_D, *a*]==0]

RESULTS AND DISCUSSION

The study investigates the mixed convective instability of Jeffrey nanofluid flow through a horizontal porous layer using a generalized eigenvalue problem both analytically and numerically. Both one-term and higher-order Galerkin methods are adapted and the obtained results are presented. By assessing the convergence process by increasing the number of terms N in the Galerkin expansion. The process of convergence of WGRM is shown in Table 2-4 for various values of governing parameters involved therein. It is noted that the convergence of the critical Darcy-Rayleigh number, the corresponding critical wave number and the critical frequency is accomplished by considering ten terms in WGRM. We have thoroughly examined and established the convergence and validity of our numerical method. To validate the numerical procedure employed, the results are computed under the limiting case and observe that they are in excellent agreement.

A glance at Tables 2-4 shows that there is not much deviation in the values of critical stability parameters between the second (N = 2) and higher order (N =10) (WGRM). Thus it is intuitive to look for the analytical solution for the eigenvalue problem with $\Psi = A\sin\pi z$ and $\Theta = B\sin\pi z$ as basis functions for the solutions of equations (20) and (21).

Table 2. Convergence of the WRGM for different values of Π with $\varphi = 0.025$ for TiO_2 nanoparticles

$\alpha_1 = 10, q_1 = 0.97, \Lambda = 0.5, V_a = 2$									
	Π = 2			Π = 5			Π = 10		
N	R_{Dc}	a_c	ω_{ic}	R_{Dc}	a_c	ω_{ic}	R_{Dc}	a_c	ω_{ic}
2	220.2016	2.8283	0.0165	221.6212	2.8282	0.0413	226.6909	2.8277	0.0826
3	293.5132	3.2659	0.0124	294.9386	3.2658	0.0310	300.0294	3.2655	0.0621
4	270.3464	3.1342	0.0134	271.7703	3.1341	0.0337	276.8556	3.1337	0.0674
5	271.5368	3.1412	0.0134	272.9608	3.1410	0.0335	278.0465	3.1407	0.0671
6	271.6027	3.1415	0.0134	273.0267	3.1414	0.0335	278.1124	3.1410	0.0671
7	271.6013	3.1415	0.0134	273.0253	3.1414	0.0335	278.1109	3.1410	0.0671
8	271.6005	3.1415	0.0134	273.0245	3.1414	0.0335	278.1102	3.1410	0.0671
9	271.6005	3.1415	0.0134	273.0245	3.1414	0.0335	278.1102	3.1410	0.0671
10	271.6005	3.1415	0.0134	273.0245	3.1414	0.0335	278.1102	3.1410	0.0671
One term	271.6005	3.1415	0.0134	273.0245	3.1414	0.0335	278.1102	3.1410	0.0671

Table 3. Convergence of the WRGM for different values of Π with $\varphi = 0.075$ for TiO_2 nanoparticles

$\alpha_1 = 9.9075, q_1 = 0.9387, \Lambda = 0.5, V_a = 2$									
	Π = 2			Π = 5			Π = 10		
N	R_{Dc}	a_c	ω_{ic}	R_{Dc}	a_c	ω_{ic}	R_{Dc}	a_c	ω_{ic}
2	225.4444	2.8284	0.0166	226.9247	2.8282	0.0417	232.2116	2.8276	0.0834
3	300.4997	3.2659	0.0125	301.9862	3.2658	0.0313	307.2953	3.2654	0.0626
4	276.7819	3.1342	0.0136	278.2668	3.1341	0.0340	283.5701	3.1337	0.0680
5	278.0006	3.1412	0.0135	279.4857	3.1410	0.0338	284.7893	3.1406	0.0677
6	278.0681	3.1415	0.0135	279.5531	3.1414	0.0338	284.8568	3.1410	0.0677
7	278.0666	3.1415	0.0135	279.5517	3.1414	0.0338	284.8553	3.1410	0.0677
8	278.0658	3.1415	0.0135	279.5509	3.1414	0.0338	284.8546	3.1410	0.0677
9	278.0659	3.1415	0.0135	279.5509	3.1414	0.0338	284.8546	3.1410	0.0677
10	278.0659	3.1415	0.0135	279.5509	3.1414	0.0338	284.8546	3.1410	0.0677
One term	278.0659	3.1415	0.0135	279.5509	3.1414	0.0338	284.8546	3.1410	0.0677

Table 4. Convergence of the WRGM for different values of Π with φ = 0.1 for TiO_2 nanoparticles

$\alpha_1 = 9.8113, q_1 = 0.9182, \Lambda = 0.5, V_a = 1$									
	Π = 2			Π = 5			Π = 10		
N	R_{Dc}	a_c	ω_{ic}	R_{Dc}	a_c	ω_{ic}	R_{Dc}	a_c	ω_{ic}
2	51.5339	2.8283	0.0073	53.6886	2.8277	0.0215	252.8123	2.8255	0.0531
3	321.0950	3.2659	0.0067	328.3130	3.2655	0.0112	246.6625	3.2640	0.0324
4	277.9293	3.1342	0.0071	280.1310	3.1337	0.0138	285.4222	3.1321	0.0378
5	271.0724	3.1411	0.0069	283.2749	3.1406	0.0137	288.5694	3.1390	0.0375
6	281.2463	3.1416	0.0069	283.4489	3.1410	0.0137	288.7436	3.1394	0.0375
7	281.2426	3.1416	0.0069	283.4451	3.1410	0.0137	288.7398	3.1394	0.0375
8	281.4914	3.1416	0.0069	283.0340	3.1415	0.0171	288.5467	3.1413	0.0343
9	281.4914	3.1416	0.0069	283.0340	3.1415	0.0171	288.5467	3.1413	0.0343
10	281.4914	3.1416	0.0069	283.0340	3.1415	0.0171	288.5467	3.1413	0.0343
One term	281.4914	3.1416	0.0069	283.0340	3.1415	0.0171	288.5467	3.1413	0.0343

By substituting these into Equations (20) and (21), we can express them in the matrix form as follows:

$$\begin{bmatrix} \left(\frac{1}{1+\Lambda}-\frac{ia\omega}{V_a}\right)\delta^2 & iaq_1R_D \\ ia & -\alpha_1\delta^2-i\Pi a+ia\omega \end{bmatrix}\begin{bmatrix}\Psi\\ \Theta\end{bmatrix}=\begin{bmatrix}0\\0\end{bmatrix} \quad (31)$$

where, $\delta^2 = a^2 + \pi^2$.

Equation (31) represents a homogeneous system and for a non-trivial solution, we should have

$$\begin{vmatrix} \left(\frac{1}{1+\Lambda}-\frac{ia\omega}{V_a}\right)\delta^2 & iaq_1R_D \\ ia & -\alpha_1\delta^2-i\Pi a+ia\omega \end{vmatrix}=0 \quad (32)$$

Solving this determinant for R_D, we get

$$R_D=\frac{\delta^2\left\{iV_a+a(1+\Lambda)\omega\right\}\left[-i\delta^2\alpha_1+(\Pi-\omega)a\right]}{a^2q_1V_a(1+\Lambda)} \quad (33)$$

After rearranging this expression, it is represented in a complex form as follows,

$$R_D=\Delta_1+i\omega\,\Delta_2 \quad (34)$$

where

$$\Delta_1=\frac{\delta^2\left[\pi^2V_a\alpha_1+a^2\left\{V_a\alpha_1-(1+\Lambda)(\Pi-\omega_i)\omega_i\right\}\right]}{a^2q_1V_a(1+\Lambda)}, \quad (35)$$

$$\Delta_2=\frac{a\delta^2\left[V_a(\Pi-\omega_i)+\delta^2\alpha_1(1+\Lambda)\omega_i\right]}{a^2q_1V_a(1+\Lambda)}. \quad (36)$$

Since R_D is a physical quantity, we take $\Delta_2 = 0$ ($\omega_i \neq 0$) in Eq. (34) and this gives a dispersion relation of the form:

$$b_1\omega_i+b_0=0. \quad (37)$$

where,

$$b_1 = aV_a\,\delta^2\,\Pi,$$

$$b_0 = -aV_a\,\delta^2+\alpha_1\delta^4(1+\Lambda).$$

Equation (37) reveals that for an appropriate combination of the governing parameters Π, q_1, α_1, Λ, and V_a. The minimum value of R_D and ω_i over the wave number a is numerically found for several values of controlling parameters. The results so obtained are also given in Table 2-4 in the last row and the results are in excellent agreement with those computed numerically from WGRM.

The equation (34) suggests that the preferred mode is always oscillatory. Thus, for a Newtonian fluid, $q_1 = 1$ and $\alpha_1 = 1$ then equation (33) reduces to

$$R_D=\frac{\delta^2\left\{-iV_a+a(1+\Lambda)\omega\right\}\left\{i\delta^2+a(\omega-\Pi)\right\}}{a^2V_a(1+\Lambda)} \quad (38)$$

The above expression in the equation (38), with $\Pi = 0$ and $\omega = 0$, subsequently reducing to

$$R_D=\frac{\delta^4}{a^2(1+\Lambda)} \quad (39)$$

This expression matches with [35] and represents the onset of stationary convection limiting the case to LTE. The above expression is in the equation (39) with $\Lambda = 0$ which coincides with Horton and Rogers, Lapwood's Problem.

$$R_{Dc}=\frac{\delta_c^{\,4}}{a_c^{\,2}}. \quad (40)$$

Analysis of the Growth Rate

The critical wave number and growth rate ω_i are plotted in Figures 2-5 for various values of R_D, Λ, Π and different nanoparticles. The growth rate helps us comprehend the onset of instability in the (a, ω_i)plane. The sign of ω_i determines the stability of the system: if $\omega_i < 0$, the system is stable, and if $\omega_i > 0$, it is unstable. Figure 2 shows a plot for TiO_2 ($\alpha_1 = 10$, $q_1 = 0.97$) nanoparticles with $\Pi = 2$, $\Lambda = 0.3$ and $V_a = 1$ for various values of R_D. We observe that the curve starts from a negative value and remains negative for lower values of R_D signifying that the base flow is always linearly stable, and for higher values of R_D the sign of ω_i changes from negative to positive indicating the possibility of the flow becoming unstable. In Figure 3, for $R_D = 250$, ω_i is positive for $\Lambda = 0.9$ and 0.7, indicating the occurrence of

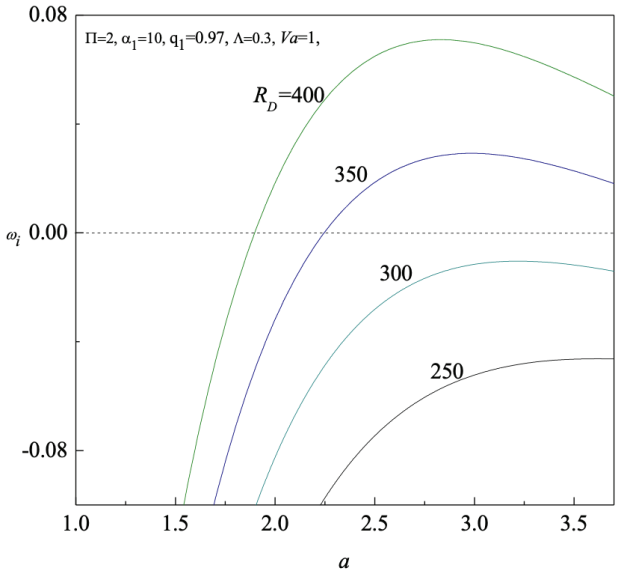

Figure 2. Growth rate ω_{ic} versus wavenumber a for different values of R_D.

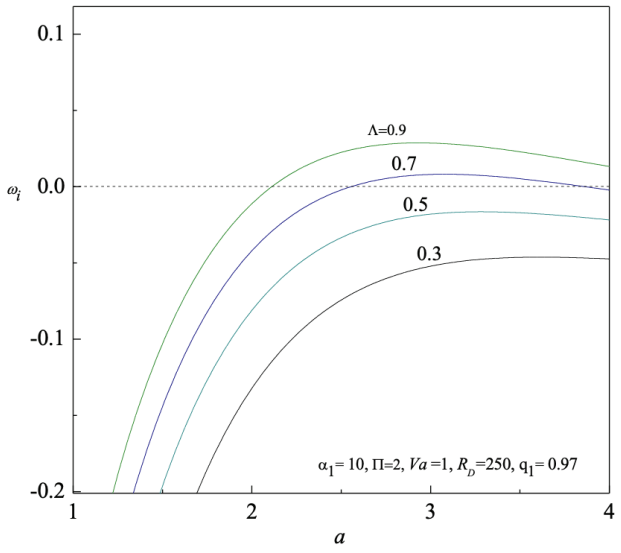

Figure 3. Growth rate ω_i versus wavenumber a for different values of Λ.

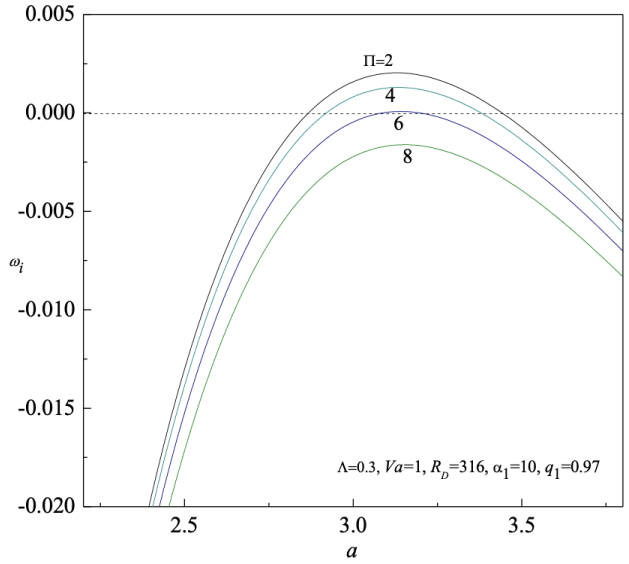

Figure 4. Growth rate ω_i versus wavenumber a for different values of Π.

transition from stability to instability for all considered values, whereas for Λ = 0.3 and 0.5, it is stable. In Figure 4, by varying Π with R_D = 316, while keeping other parameters fixed as mentioned above, it is observed that the fluid flow for Π = 2, 4, 6 enters the positive regime of ω_i indicating the onset of instability, while for Π = 8 the curve passes through the maximum in the negative region of ω_i ensuring the stability of the flow. A significant change in the curve's behavior is observed when considering different nanoparticles (Fig. 5). Specifically, TiO_2 and Al_2O_3 particles show

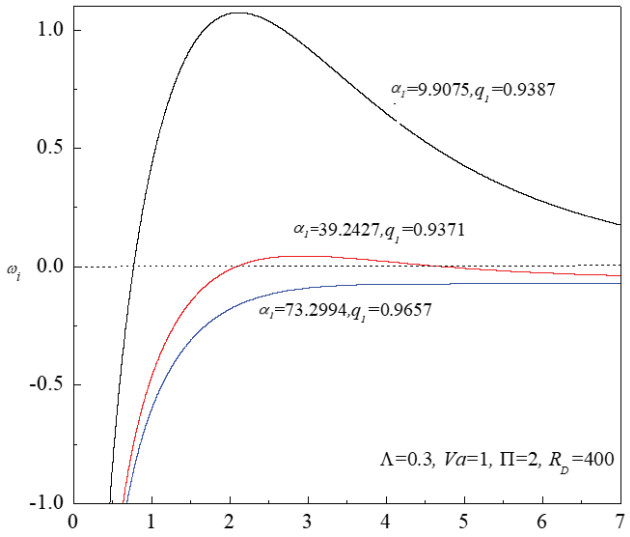

Figure 5. Growth rate ω_i versus wavenumber a for different nanoparticles.

instability, while CuO particles remain stable for the considered parametric values.

Neutral Stability Curves

The neutral stability curves presented in Figures 6-9 depict the relationship between the Darcy-Rayleigh number (R_D) and a wave number (a) in (a, R_D)-plane by considering various physical parameters, including the Jeffrey parameter, horizontal pressure gradient, Vadasz number, thermal diffusivity ratio, and different nanoparticle ratios. These curves exhibit a uni-modal nature similar to those observed in classical Darcy–Bénard problems, indicating the occurrence of a single mode of convection. Upon closer analysis of the graphs, several vital observations emerge. Figure 6 shows that an increase in the Jeffrey parameter is a decrease in the stability region. Similar behavior could be seen with an increasing Vadasz number (Fig. 9). This phenomenon can be attributed to the higher fluid viscosity associated with increased Jeffrey parameter and Vadasz number, which impedes fluid motion and destabilizes the system. Conversely, an increase in the horizontal pressure gradient (Fig. 7) leads to an expansion of the stability region. This is due to the increased driving force exerted on the fluid, which enhances fluid motion and promotes stability. Furthermore, Figure 8 reveals that a decrease in the Darcy-Rayleigh number due to nanoparticle ratios reduces the stability region. This can be attributed to the nanofluid's altered thermal conductivity and viscosity caused by the type of nanoparticles, leading to changes in convective heat transfer and fluid flow patterns. Moreover, an increase in the Jeffrey parameter and nanoparticle ratios is observed to destabilize the system, as indicated by the reduction in the stability region. This destabilization can be attributed to the nanofluid's increased viscosity and altered thermal

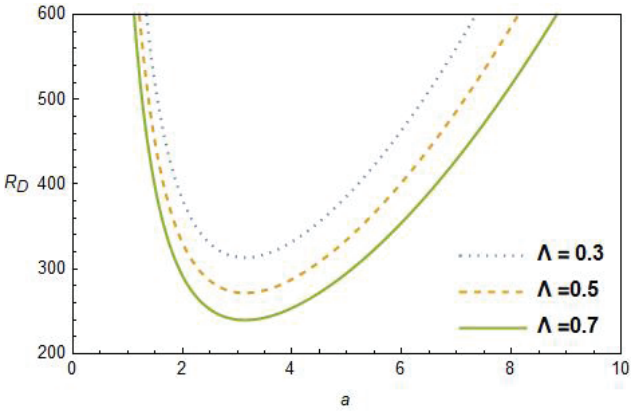

Figure 6. Neutral Stability curves for different values of Λ with $\alpha_1 = 10$, $q_1 = 0.97$, Π = 2 and $V_a = 1$.

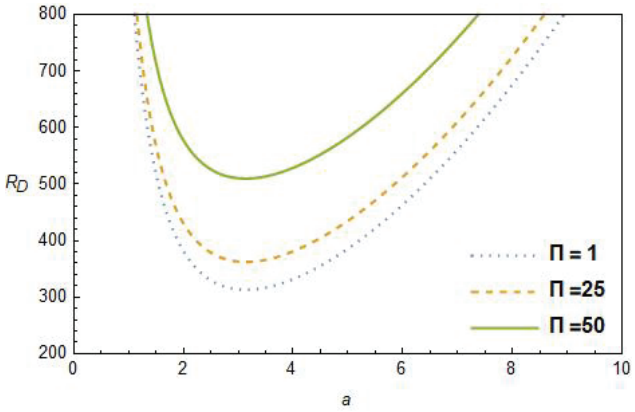

Figure 7. Neutral Stability curves for different values of Π with $\alpha_1 = 10$, $q_1 = 0.97$, $V_a = 1$ and Λ = 0.3.

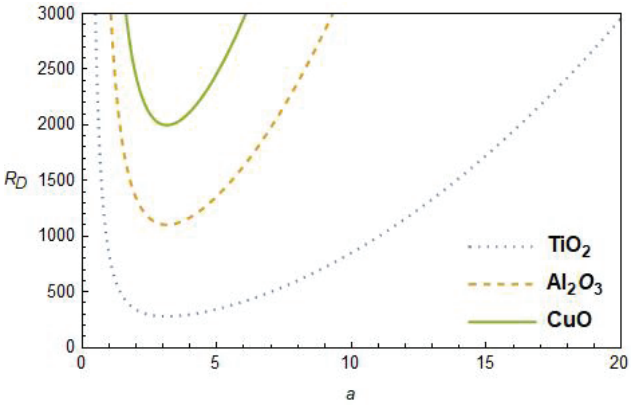

Figure 8. Neutral Stability curves for different nanoparticles with, ϕ = 0.075, Π = 5, Va = 1 and Λ = 0.5.

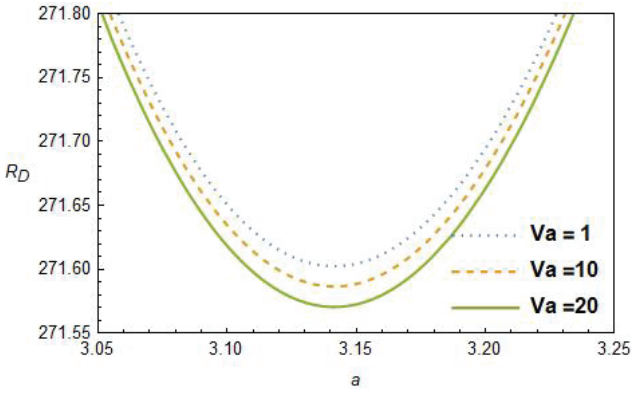

Figure 9. Neutral Stability curves for different values of V_a with $\alpha_1 = 10$, $q_1 = 0.97$, Π = 2 and Λ = 0.5.

properties, which disrupt fluid flow and convective heat transfer processes.

Additionally, Figure 8 demonstrates the comparative stability of water-CuO, water- Al_2O_3 and water TiO_2 nanofluids. It suggests that CuO dispersed in water exhibits more excellent stability than water- Al_2O_3 and water TiO_2 nanofluid, primarily due to the differences in thermal conductivity and thermal sensitivity of the nanoparticles. Specifically, CuO nanoparticles contribute to enhanced heat transfer and stability, whereas water TiO_2 and Al_2O_3 nanofluids display instability owing to its higher thermal sensitivity, which can lead to thermal fluctuations and convective instability. In summary, the findings from the neutral stability curves provide valuable insights into the complex interplay between various parameters and their effects on the stability of Jeffrey nanofluid flow through porous media. These insights contribute to a deeper understanding of the underlying mechanisms governing convective behavior and have implications for designing and optimizing thermal management systems in various engineering applications.

Critical Curves

The behavior of R_{Dc}, a_c, and ω_{ic} as functions of Π is elucidated in Figures 10-12 for different values of the Jeffrey parameter Λ, specifically Λ = 0.3, Λ = 0.5, and Λ = 0.7. Figure (10) shows that the critical Darcy-Rayleigh number R_{Dc} remains invariant for small values of Π, indicating a stable regime. However, beyond Π > 2, Π starts to influence R_{Dc}, increasing its increase. Additionally, an increase in the Jeffrey parameter Π is noted to decrease the critical Darcy-Rayleigh number R_{Dc}, thereby advancing the onset of convection. Figure 11 shows that the critical wave number a_c decreases with rising values of Π, consequently diminishing the size of the convection cells. Conversely, in Figure 12, the necessary frequency ω_{ic} decreases with increasing Π values, indicating a stabilizing effect, while it increases with rising Π, suggesting enhanced oscillatory behavior.

Similarly, the behavior of R_{Dc}, a_c, and ω_{ic} as functions of Π are explored in Figures 13-15 for different values of the Vadasz number V_a, specifically $V_a = 1$, $V_a = 10$, and $V_a = 20$. In Figure 13, it is observed that in the critical Darcy-Rayleigh number R_{Dc}, the effect of small Π values are

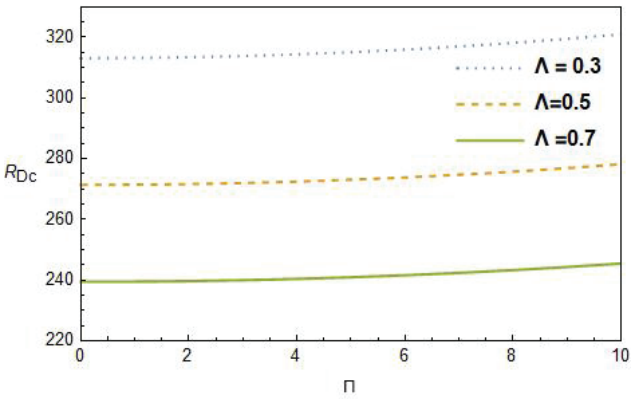

Figure 10. Critical curves of Darcy-Rayleigh number as a function of Π for different values of Λ with $\alpha_1 = 10$, $q_1 = 0.97$, and $V_a = 1$.

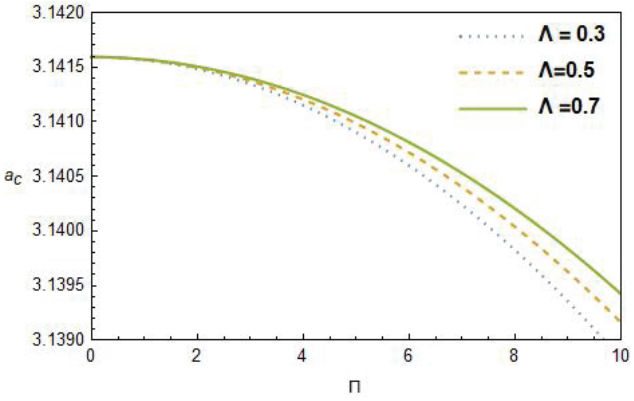

Figure 11. Critical curves of wave number as a function of Π for different values of Λ with $\alpha_1 = 10$, $q_1 = 0.97$ and $V_a = 10$.

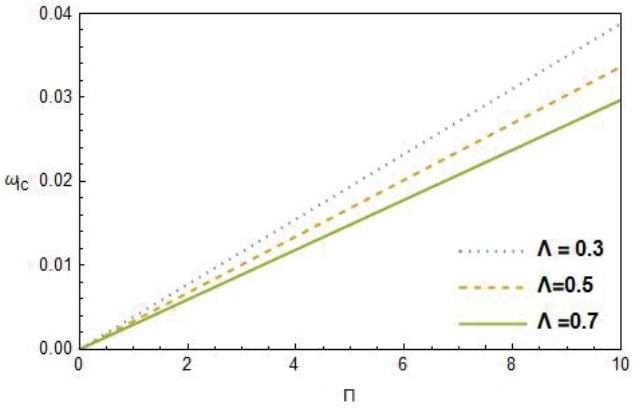

Figure 12. Critical curves of wave frequency as a function of Π for different values of Λ with $\alpha_1 = 10$, $q_1 = 0.97$ and $V_a = 1$.

negligible but start to increase beyond Π = 1, signifying the influence of Π on R_{Dc} and subsequent destabilization. Moreover, an increase in V_a is observed to expand the stability region, thus delaying the onset of convection. Figure 14 shows that the critical wave number a_c decreases with an increase in V_a and Π values, leading to a reduction in the size of convection cells. Finally, in Figure 15, the critical frequency ω_{ic} is seen to increase with increasing Π values, while it increases with increasing V_a, reflecting the system's response to changes in flow parameters.

Further, the plots of R_{Dc}, $a_{c,}$ and ω_{ic} as functions of Λ are illustrated in Figures 16-18 for different values of V_a = 1, 10, and 20. Figure 16 reveals a linear decrease in the critical Darcy-Rayleigh number R_{Dc} with increasing Λ. Hence, it destabilizes the system. Also, a similar trend is observed with an increase in V_a. In Figure 17, an increase in Λ and V_a is seen to increase and decrease a_c, respectively, leading to changes in the size of convection cells. Finally, in Figure 18, the values of ω_{ic} are observed to increase with increasing V_a values. In contrast, an opposite effect could be seen with an increase in Λ, indicating the system's response to variations in flow parameters.

Analysis of the data presented in Table 5 reveals a consistent trend: as the Jeffrey parameter increases, there is a notable decrease in the critical Darcy Rayleigh number

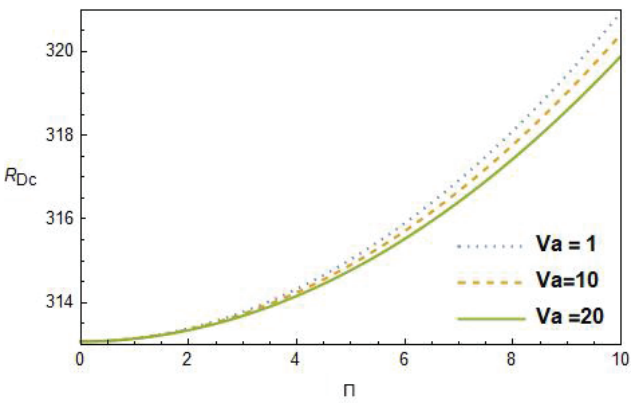

Figure 13. Critical curves of R_{Dc} Vs Π for different values of V_a with $\alpha_1 = 10$, $q_1 = 0.97$ and Λ = 0.3.

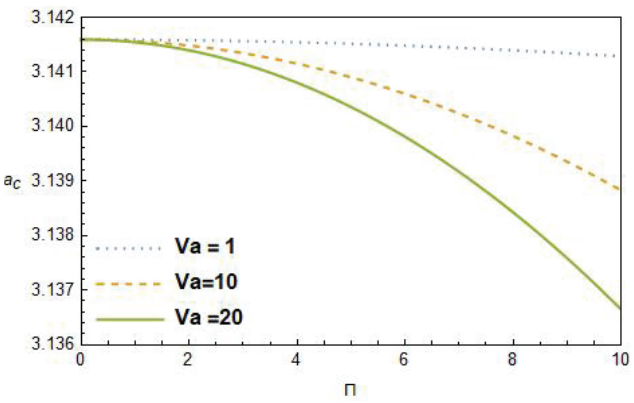

Figure 14. Critical curves of a_c Vs Π for different values of V_a with $\alpha_1 = 10$, $q_1 = 0.97$ and Λ = 0.3.

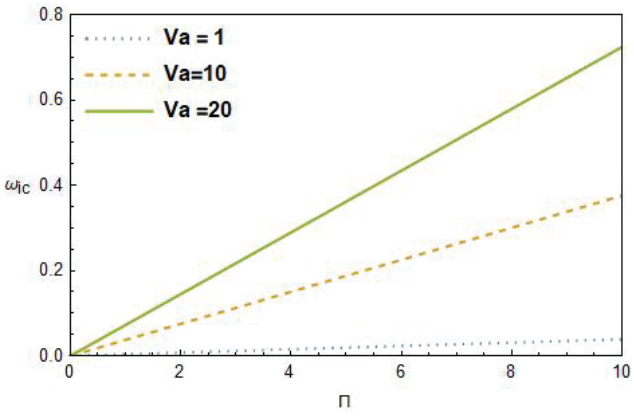

Figure 15. Critical curves of ω_{ic} Vs Π for different values of V_a with $\alpha_1 = 10$, $q_1 = 0.97$ and $\Lambda = 0.3$.

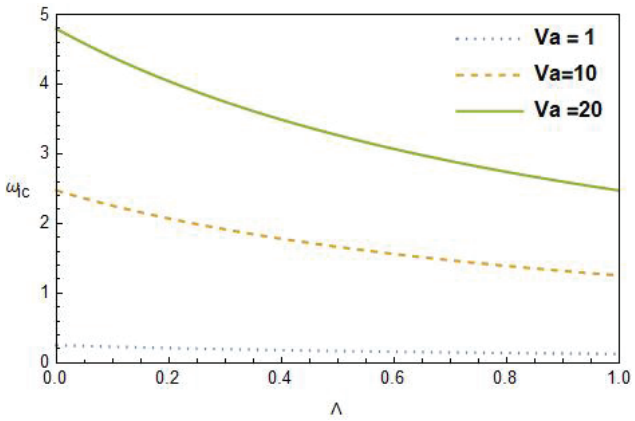

Figure 18. Critical curves of ω_{ic} Vs Λ for different values of V_a with $\Pi = 5$, $V_a = 2$ and $\Pi = 50$.

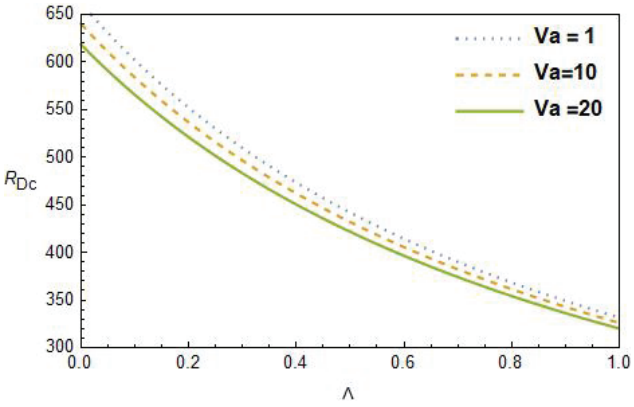

Figure 16. Critical curves of R_{Dc} Vs Λ for different values of V_a with $\alpha_1 = 10$, $q_1 = 0.97$ and $\Pi = 50$.

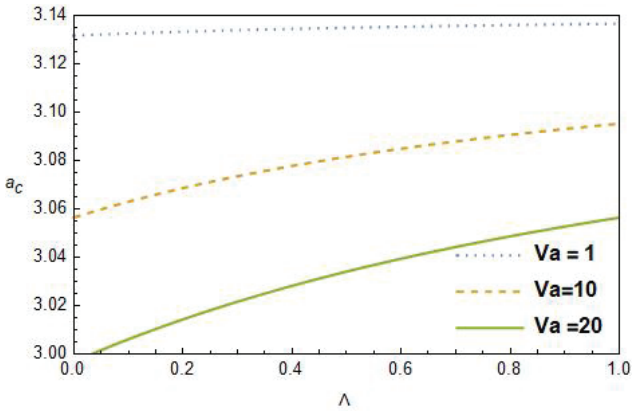

Figure 17. Critical curves of a_c Vs Λ for different values of V_a with $\Pi = 5$, $V_a = 2$ and $\Pi = 50$.

Table 5. Critical values of R_{Dc}, a_c and ω_{ic} for different combinations of nanoparticles and Jeffrey parameter

	CuO ($V_a = 2$, $\Pi = 5$) $\alpha_1 = 73.2993$, $q_1 = 0.9657$ $\varphi = 0.075$			**Al_2O_3 ($V_a = 2$, $\Pi = 5$) $\alpha_1 = 39.2427$, $q_1 = 0.9371$ $\varphi = 0.075$**			**TiO_2 ($V_a = 2$, $\Pi = 5$) $\alpha_1 = 9.9075$, $q_1 = 0.9387$ $\varphi = 0.075$**		
Λ	R_{Dc}	a_c	ω_{ic}	R_{Dc}	a_c	ω_{ic}	R_{Dc}	a_c	ω_{ic}
0	2996.8773	3.14159	0.00690	1653.90400	3.14158	0.012876	419.30855	3.14139	0.050619
0.3	2305.2904	3.14159	0.00531	1272.23450	3.14159	0.009910	322.55454	3.14143	0.039028
0.5	1997.9184	3.14159	0.00460	1102.60350	3.14159	0.008591	279.55094	3.14145	0.033859
0.7	1762.8692	3.14159	0.00406	972.88558	3.14159	0.007582	246.66508	3.14147	0.029899
0.9	1577.3041	3.14159	0.00363	870.47668	3.14159	0.006785	220.70210	3.14148	0.026769

across all three types of nanoparticles under examination. This suggests that higher Jeffrey parameters enhance these nanofluids convective stability. Specifically, when focusing on CuO nanoparticles, it becomes apparent that they exhibit a maximal critical Darcy and Rayleigh number compared to the other nanoparticle types. This maximal value indicates that CuO nanoparticles possess superior thermal stability relative to their counterparts. On the other hand, the wave frequency demonstrates a contrasting behavior. Across all nanoparticle types, there is a discernible decrease in wave frequency. Notably, Al_2O_3 nanoparticles exhibit the highest frequency among the studied particles. Drawing insights from these observations, it can be inferred that the onset of convection varies across the different nanoparticles. For

Al_2O_3 nanoparticles, the onset of convection appears to be at an intermediate stage. In contrast, for TiO_2 nanoparticles, convection onset occurs more rapidly. Interestingly, for CuO nanoparticles, the onset of convection unfolds much more gradually compared to the other nanoparticle types. These nuanced distinctions in convection onset further underscore the complex interplay between nanoparticle characteristics and fluid dynamics.

CONCLUSION

In this study, we performed a thorough stability analysis of mixed convective flow with a volume fraction of Jeffrey nanofluid in a porous layer, using both numerical and analytical methods. The study utilized the unsteady Jeffrey-Darcy model, which includes the Jeffrey parameter to address retardation or relaxation effects. This model is particularly well-suited for situations involving low-volume fraction Jeffrey nanoparticles and porous layers with low permeability. Specifically, we utilized the Weighted Residual Galerkin Method (WRGM) for numerical analysis and the one-term Galerkin method for analytical investigation. It is shown that the results are in good agreement with N=8. Also, the growth rate of perturbations is numerically computed over a broad spectrum of governing parameters, revealing a notable change in the growth rate behavior for TiO_2 and Al_2O_3 particles, exhibiting instability, while CuO particles remain stable within the considered parametric range. Some of the important results of this analysis can be outlined as follows:

1. The neutral stability curves exhibit a single minimum, and we observe that the instability region diminishes with increasing nanoparticle volume fraction in the base fluid. This phenomenon suggests that higher volume fractions result in amplified resistance to flow.
2. Increasing Π leads to an expansion of the stability region, indicating a stabilizing effect. Conversely, an increasing value of the Jeffrey parameter Λ results in a contraction of the stability region for all nanoparticles, implying a destabilizing influence.
3. Increasing the Vadasz number is to decrease the Darcy-Rayleigh number hence advances the onset of convection.
4. An increase in the Jeffrey parameter Λ tends to decrease the critical values of R_{Dc} and ω_{ic}, accelerating the initiation of convective activity. However, a_c exhibits a reverse trend, decreasing a_c value with an increase of Λ for all nanofluids, indicating a stabilizing effect on convective cell size.
5. We observe that the Jeffrey parameter Λ can act as both a stabilizer and a destabilizer, depending on its combination with other parameters, highlighting its versatile role in influencing convective stability. These conclusions provide valuable insights into the complex interplay of parameters affecting the stability of mixed convective flow in Jeffrey nanofluids through porous media, contributing to a deeper understanding of thermal transport phenomena in such systems.
6. The critical Darcy-Rayleigh number for various nanoparticles exhibits an inequality of the form $\left(R_{Dc}\right)_{CuO} > \left(R_{Dc}\right)_{Al_2O_3} > \left(R_{Dc}\right)_{TiO_2}$.

To develop for further analysis, one challenge is to investigate the non-linear instability analysis, while the paper will also explore extending the present work by considering the solute concentration and heat source.

NOMENCLATURE

$\vec{q}$	Dimensional velocity vector
t	Time
P	Pressure
K	Permeability of porous medium
d	Length of channel
(x, z)	Dimensional coordinates
C	Specific heat at constant pressure
$\vec{g}$	Gravitational acceleration
T	Temperature
k	Thermal conductivity
R_D	Darcy-Raleigh Number
V_a	Vadasz Number
$q_1 = \frac{\rho_{nf}\beta_{nf}}{\rho_{bf}\beta_{bf}}$	Nanoparticle volume fraction parameter.

Greek symbols

λ	Jeffrey parameter
ϕ	Nanoparticle volume fraction
ρ_0	Reference density of fluid
ρ	Density of fluid
β	Volumetric expansion coefficient
α	Thermal diffusivity
$\alpha_1 = \frac{\alpha_{nf}}{\alpha_f}$	The ratio of thermal diffusivities.
μ	Viscosity of the nanofluid
ε	Porosity
σ	heat capacity ratio
Λ	Non-dimensional Jeffrey parameter
Π	Constant horizontal pressure gradient

Subscripts

p	Nanoparticle
nf	Nanofluid
bf	Base fluid
c	Cold
h	Hot

ACKNOWLEDGMENT

We extend our appreciation to Anonymous Reviewers for their input and suggestions which have played a crucial role in improving the overall quality of the manuscript also the authors are thankful to the authorities of their respective institutions for encouragement and support in carrying

out this research work. All the authors acknowledge the support of Visvesvaraya Technological University as well.

AUTHORSHIP CONTRIBUTIONS

Authors equally contributed to this work.

DATA AVAILABILITY STATEMENT

The authors confirm that the data that supports the findings of this study are available within the article. Raw data that support the finding of this study are available from the corresponding author, upon reasonable request.

CONFLICT OF INTEREST

The authors declared no potential conflicts of interest with respect to the research, authorship, and/or publication of this article.

ETHICS

There are no ethical issues with the publication of this manuscript.

FUNDING

This research work is funded by BMSCE under the FRP scheme with a project No. R&D/FRPS/2022-23/MAT/02.

REFERENCES

[1] Prasad V, Lai FC, Kulacki FA. Mixed convection in horizontal porous layers heated from below. J Heat Transf 1988;395–402. [CrossRef]

[2] Sphaier LA, Barletta A. Unstable mixed convection in a heated horizontal porous channel. Int J Therm Sci 2014;78:77–89. [CrossRef]

[3] Ozgen F, Varol Y. Numerical study of mixed convection in a channel filled with a porous medium. Appl Sci 2019;9:211. [CrossRef]

[4] Vafai K. Handbook of Porous Media. New York: CRC Press; 2005. [CrossRef]

[5] Kim Y, Vafai K. Buoyancy-driven heat transfer enhancement in a two-dimensional porous enclosure utilizing nanofluids. Int J Heat Mass Transf 2006;49:2402–2414.

[6] Abu-Nada E, Chamkha AJ. Mixed convection flow in a lid-driven cavity filled with a fluid-saturated porous medium: effect of a conducting vertical solid plate on the left wall. Int J Heat Mass Transf 2007;50:727–735.

[7] Nield DA, Bejan A. Convection in Porous Media. New York: Springer; 2006.

[8] Ingham DB, Pop I. Transport Phenomena in Porous Media III. Amsterdam: Elsevier; 2013.

[9] Nield DA. A note on a porous medium model with the Navier slip boundary condition. Int J Heat Mass Transf 2013;62:287–291.

[10] Postelnicu A. The effect of a horizontal pressure gradient on the onset of a Darcy-Bénard convection in thermal non-equilibrium conditions. Int J Heat Mass Transf 2010;53:68–75. [CrossRef]

[11] Buongiorno J. Convective transport in nanofluids. ASME J Heat Transf 2005;128:240–250. [CrossRef]

[12] Choi SU, Zhang ZG, Yu W, Lockwood FE, Grulke EA. Anomalous thermal conductivity enhancement in nanotube suspensions. Appl Phys Lett 2019;79:2252–2254. [CrossRef]

[13] R Mostafizur RM, Saidur R, Abdul Aziz AR, Bhuiyan MHU. Thermophysical properties of methanol-based Al_2O_3 nanofluids. Int J Heat Mass Transf 2015;85:414–419. [CrossRef]

[14] Tzou DY. Thermal instability of nanofluids in natural convection. Int J Heat Mass Transf 2008;51:2967–2979. [CrossRef]

[15] Nield DA, Kuznetsov AV. Thermal instability in a porous medium layer saturated by a nanofluid. Int J Heat Mass Transf 2009;52:5796–5801. [CrossRef]

[16] Kuznetsov AV, Nield DA. Effect of local thermal non-equilibrium on the onset of convection in a porous medium layer saturated by a nanofluid. Transp Porous Media 2010;83:425–436. [CrossRef]

[17] Bhadauria BS, Agarwal S. Convective transport in a nanofluid saturated porous layer with thermal nonequilibrium model. Transp Porous Media 2011;88:107–131. [CrossRef]

[18] Chand R, Rana GC. Oscillating convection of nanofluid in a porous medium. Transp Porous Media 2012;95:269–284. [CrossRef]

[19] Yadav D, Agrawal GS, Bhargava R. The onset of convection in a binary nanofluid saturated porous layer. Int J Theor Appl Multiscale Mech 2012;2:198–224. [CrossRef]

[20] Yadav D, Mohamed R, Lee J, Cho HH. Thermal convection in a Kuvshiniski viscoelastic nanofluid saturated porous layer. Ain Shams Eng J 2017;8:613–621. [CrossRef]

[21] Sheu LJ. Linear stability of convection in a viscoelastic nanofluid layer. World Acad Sci Eng Technol Int J Mech Mechatron Eng 2011;5:1970–1976.

[22] Chand R, Rana GC, Puigjaner D. Thermal instability analysis of an elastic-viscous nanofluid layer. Eng Trans 2018;66:301–324.

[23] Zangooee MR, Hosseinzadeh K, Ganji DD. Hydrothermal analysis of Ag and CuO hybrid NPs suspended in a mixture of water 20%+ EG 80% between two concentric cylinders. Case Stud Therm Eng 2023;50:103398. [CrossRef]

[24] Alipour N, Jafari B, Hosseinzadeh K. Optimization of the wavy trapezoidal porous cavity containing a mixture of hybrid nanofluid (water/ethylene glycol Go–Al_2O_3) by response surface method. Sci Rep 2023;13:1635. [CrossRef]

[25] Hosseinzadeh K, Mardani MR, Paikar M, Hasibi A, Tavangar T, Nimafar M, et al. Investigation of second-grade viscoelastic non-Newtonian nanofluid flow on the curve stretching surface in the presence of MHD. Results Eng 2023;17:100838. [CrossRef]
[26] Fallah Najafabadi M, Talebi Rostami H, Hosseinzadeh K, Ganji DD. Hydrothermal study of nanofluid flow in the channel by RBF method with exponential boundary conditions. Proc Inst Mech Eng E 2023;237:2268–2277. [CrossRef]
[27] Faghiri S, Akbari S, Shafii MB, Hosseinzadeh K. Hydrothermal analysis of non-Newtonian fluid flow (blood) through the circular tube under prescribed non-uniform wall heat flux. Theor Appl Mech Lett 2022;12:100360. [CrossRef]
[28] Zangooee MR, Hosseinzadeh K, Ganji DD. Hydrothermal analysis of hybrid nanofluid flow on a vertical plate by considering slip condition. Theor Appl Mech Lett 2022;12:100357. [CrossRef]
[29] Akbari S, Faghiri S, Poureslami P, Hosseinzadeh K, Shafii MB. Analytical solution of non-Fourier heat conduction in a 3-D hollow sphere under time-space varying boundary conditions. Heliyon 2022;8:e12496. [CrossRef]
[30] Attar MA, Roshani M, Hosseinzadeh K, Ganji DD. Analytical solution of fractional differential equations by Akbari–Ganji's method. Partial Differ Equ Appl Math 2022;6:100450. [CrossRef]
[31] Mahboobtosi M, Hosseinzadeh K, Ganji DD. Entropy generation analysis and hydrothermal optimization of ternary hybrid nanofluid flow suspended in polymer over a curved stretching surface. Int J Thermofluids 2023;20:100507. [CrossRef]
[32] Talebi Rostami H, Fallah Najafabadi M, Hosseinzadeh K, Ganji DD. Investigation of mixture-based dusty hybrid nanofluid flow in porous media affected by magnetic field using RBF method. Int J Amb Energy 2022;43:6425–6435. [CrossRef]
[33] Nadeem S, Akbar NS. Peristaltic flow of a Jeffrey fluid with variable viscosity in an asymmetric channel. Z Naturforsch A 2009;64:713–722. [CrossRef]
[34] Nallapu S, Radha Krishnamacharya G, Chamkha AJ. Flow of a Jeffrey fluid through a porous medium in narrow tubes. J Porous Media 2015;18:71–78. [CrossRef]
[35] Yadav D. Influence of anisotropy on the Jeffrey fluid convection in a horizontal rotary porous layer. Heat Transf 2021;50:4595–4606. [CrossRef]
[36] Naganthran K, Nazar R, Pop I. Effects of heat generation/absorption in the Jeffrey fluid past a permeable stretching/shrinking disc. J Braz Soc Mech Sci Eng 2019;41:414. [CrossRef]
[37] Zhang J, Zheng L, Zhang X, Fang T. Free convection in Jeffrey nanofluid flow in a porous medium with convective boundary condition. Int J Heat Mass Transf 2018;116:240–248.
[38] Siddiqui AM, Haq RU, Khan MI. Effects of Darcy and Prandtl numbers on unsteady heat transfer of Jeffrey nanofluid through a porous medium. Eng Sci Technol Int J 2021;24:113–123.
[39] Sharma P, Kumar A, Bains D, Lata P, Rana G. Thermal convective instability in a Jeffrey nanofluid saturating a porous medium: Rigid-rigid and rigid-free boundary conditions. Struct Integ Life 2024;23:351–356.
[40] Pushap PLS, Bains D, Lata P. Thermal instability of rotating Jeffrey nanofluids in porous media with variable gravity. J Niger Soc Phys Sci 2023;5:1366. [CrossRef]
[41] Gautam PK, Rana GC, Saxena H. Stationary convection in the electrohydrodynamic thermal instability of Jeffrey nanofluid layer saturating a porous medium: Free-free, rigid-free, and rigid-rigid boundary conditions. J Porous Media. 2020;23:1043. [CrossRef]
[42] Shehzad SA, Hayat T, Alsaedi A. MHD flow of Jeffrey nanofluid with convective boundary conditions. J Braz Soc Mech Sci Eng 2015;37:873–883. [CrossRef]
[43] Shahzad F, Sagheer M, Hussain S. Numerical simulation of magnetohydrodynamic Jeffrey nanofluid flow and heat transfer over a stretching sheet considering Joule heating and viscous dissipation. AIP Adv 2018;8:065316. [CrossRef]
[44] Sreelakshmi K, Sarojamma G, Murthy J, Ramana V. Homotopy analysis of an unsteady flow heat transfer of a Jeffrey nanofluid over a radially stretching convective surface. J Nanofluids 2018;7:62–71. [CrossRef]
[45] Devi J, Sharma V, Kapalta M. Electroconvection in rotating Jeffrey nanofluid saturating porous medium: Free-Free, Rigid-Free, Rigid-Rigid boundaries. J Nanofluids 2023;12:1554–1565. [CrossRef]
[46] Devi P, Rana GC, Sharma SR, Kumar S, Gautam PK. Impact of rotation on thermal instability of Darcy–Brinkman porous layer filled with a Jeffrey nanofluid. Numer Heat Transf Part A Appl 2023;2273456. [CrossRef]
[47] Sharma PL, Kumar A, Deepak D, Rana GC. Effect of magnetic field on thermosolutal convection in Jeffrey nanofluid with porous medium. Spec Top Rev Porous Media 2023;14:17–29. [CrossRef]
[48] Maatoug S, Babu KH, Deepthi VVL, Ghachem K, Raghunath K, Ganteda C, et al. Variable chemical species and thermo-diffusion Darcy–Forchheimer squeezed flow of Jeffrey nanofluid in horizontal channel with viscous dissipation effects. J Indian Chem Soc 2023;100:100831. [CrossRef]
[49] Sushma K, Sreenadh S, Dhanalakshmi P. Mixed convection flow of a Jeffrey nanofluid in a vertical channel. Middle-East J Sci Res 2017;25:950–959.
[50] Pallavi G, Hemanthkumar C, Shivakumara IS, Rushikumar B. Oscillatory Darcy-Bénard-Poiseuille mixed convection in an Oldroyd-B fluid-saturated

porous layer. In: Rushi Kumar B, Sivaraj R, Prakash J, eds. Advances in Fluid Dynamics. Lecture Notes in Mechanical Engineering. Singapore: Springer; 2021. [CrossRef]

[51] Hemanthkumar C, Shivakumara IS. Thermal instability of an Oldroyd-B fluid saturated porous layer: Implications of pressure gradient and LTNE temperatures. SN Appl Sci 2020;2:566. [CrossRef]

[52] Singh N, Khandelwal MK. Linear stability perspective on mixed convection flow of nanofluids in a differentially heated vertical channel. Int Commun Heat Mass Transf 2022;134:105989. [CrossRef]

[53] Xuan Y, Li Q. Investigation on convective heat transfer and flow features of nanofluids. J Heat Transf 2003;125:151–155. [CrossRef]

[54] Brinkman HC. The viscosity of concentrated suspensions and solutions. J Chem Phys 1952;20:571–581. [CrossRef]

[55] Maxwell JC. A treatise on electricity and magnetism. Cambridge: Cambridge University Press; 2010. [CrossRef]

[56] Khanafer K, Vafai K, Lightstone M. Buoyancy-driven heat transfer enhancement in a two-dimensional enclosure utilizing nanofluids. Int J Heat Mass Transf 2003;46:3639–3653. [CrossRef]

[57] Xuan Y, Roetzel W. Conceptions for heat transfer correlation of nanofluids. Int J Heat Mass Transf 2000;43: 3701–3707. [CrossRef]

[58] Shankar BM, Shivakumara IS. Gill's stability problem may be unstable with horizontal heterogeneity in permeability. J Fluid Mech 2022;943:A20. [CrossRef]